energies

Article

Enhanced Dynamic Performance in Hybrid Power System Using a Designed ALTS-PFPNN Controller

Kai-Hung Lu [1], Chih-Ming Hong [2,*] and Fu-Sheng Cheng [3]

1 School of Electronic and Electrical Engineering, Minnan University of Science and Technology, Quanzhou 362700, China
2 Department of Electronic Communication Engineering, National Kaohsiung University of Science and Technology, Kaohsiung 811213, Taiwan
3 Department of Electrical Engineering, Cheng-Shiu University, Kaohsiung 833301, Taiwan
* Correspondence: hung71721@nkust.edu.tw

Abstract: The large-scale, nonlinear and uncertain factors of hybrid power systems (HPS) have always been difficult problems in dynamic stability control. This research mainly focuses on the dynamic and transient stability performance of large HPS under various operating conditions. In addition to the traditional synchronous power generator, wind-driven generator and ocean wave generator, the hybrid system also adds battery energy storage system and unified power flow controller (UPFC), making the system more diversified and more consistent with the current actual operation mode of the complex power grid. The purpose of this study is to propose an adaptive least squares Petri fuzzy probabilistic neural network (ALTS-PFPNN) for UPFC installed in the power grid to enhance the behavior of HPS operation. The proposed scheme improves the active power adjustment and dynamic performance of the integrated wave power generation and offshore wind system under a large range of operating conditions. Through various case studies, the practicability and robustness of ALTS-PFPNN method are verifying it by comparison and analysis with the damping controller based on the designed proportional integral differential (PID) and the control scheme without UPFC. Time-domain simulations were performed using Matlab-Simulink to validate the optimal damping behavior and efficiency of the suggested scheme under various disturbance conditions.

Keywords: adaptive least trimmed squares petri fuzzy probabilistic neural network (ALTS-PFPNN); offshore wind power farm; ocean wave power farm; unified power flow controller (UPFC)

check for updates

Citation: Lu, K.-H.; Hong, C.-M.; Cheng, F.-S. Enhanced Dynamic Performance in Hybrid Power System Using a Designed ALTS-PFPNN Controller. *Energies* **2022**, *15*, 8263. https://doi.org/10.3390/en15218263

Academic Editor: Adolfo Dannier

Received: 29 September 2022
Accepted: 1 November 2022
Published: 4 November 2022

1. Introduction

Wind and sea wave have similar energy properties. They are renewable energy sources that are concerned at present and help to make up for the global energy shortage. The complex power control structure is a main point so as to increase the power generated and therefore the efficiency of integrated wind and ocean wave power systems. Due to the nonlinear dynamics and uncertainties usually present in integrated wind and wave power systems, the efficiency of these systems can be increased by adopting advanced control strategies [1,2].

In response to the global trend of reducing greenhouse gas emissions and saving energy, various countries have actively developed renewable energy sources, and formed a so-called smart grid by integrating with functions such as information, network and communication technology. In view of the development of smart grids, it will help to the growth and progress of sustainable energy. Based on the consensus of improving power quality, the development of intelligent energy management and control systems has become a key trend in future development. In all international regulations on power grids, regardless of the voltage level, generators are required to have the ability to change the inductive power output. This requirement is to maintain a stable grid voltage and limit dynamic voltage changes. Generally speaking, large-capacity wind turbines are parallel connection with the voltage The higher the feeder, the more expensive the insulation equipment required, and the cost also increases. With the wind power increase of capacity, the proportion of wind power in the grid gradually increases, and the high proportion and high popularity of wind and wave power generation will inevitably affect the safe and stab of power network. Since the wind and wave speed changes with the change of climate or season, the energy captured by the turbine is changed to electric energy through the electric generator and also changes with the wind and wave speed, affects the quality of the hybrid power grid. In different operation modes, the fluctuation of wind and wave speed will also have different effects on the quality of electric power. Due to the increasing capacity of wind farms around the world, the issue of the influence of wind power work and wells turbines on the power system has received increasing attention. Main objectives of this research is to study the using intelligent control through the UPFC, and installed in the composite power grid containing the offshore wind and ocean wave farm to stabilize the dynamic performance of power network operation [3].

Recently, induction generator system has proposed a fuzzy probabilistic neural network (FPNN) to improve its transient performance [4]. Because fuzzy operations have the ability to deal with uncertain language variables, and probabilistic neural networks (PNN) can continuously learn online during the control process. Therefore, a FPNN combining these two characteristics is developed. The PNN is improved from the kernel discriminant analysis in the theory and statistical method of the bayesian network, and it is also a feed-forward neural network. The adjustment process of this method is faster and there is no problem of multiple local solutions, but the execution speed is slower and the applicability is not as common as the reverse transfer type [5,6]. Petri net (PN) theory provides methods and algorithms, which can be applied directly to metabolic network modelling and analysis so as to validate the model. Moreover, PN has process modeling, variability, accessibility and a good dynamic evolution process, so the performance of FPNN's learning process can be greatly increased and improved [7–9]. Because FPNN reduces the sense of difference between fuzziness and probability through the cross influence of different types of pattern samples, it enhances the identifiability and appropriateness of the expert database of fuzzy systems. Therefore, this research combines the good dynamic evolution process of PN with the advantages of FPNN, and proposes a more robust petri fuzzy probabilistic neural network (PFPNN) to cope with the complex power grid of multi energy combined power generation. The composite power grid in this paper simulates the randomness and abruptness of real offshore wind power and wave power generation plants. Therefore, UPFC with PFPNN can effectively increase the stability and robustness of random energy changes and major faults. At present, UPFC is the most comprehensive and strongest FACTS controllers among many new FACTS controllers. It combines the control functions of series equipment and parallel equipment, so it can control local sinks at the same time [10–13]. Therefore, this study applies UPFC to the power network with multiple energy sources (wind, wave, SG and BESS) to increase the system stability under various operating conditions. To compare the transient performance improvement applied to the PFPNN control system, these results were compared with the designed PID controller. The simulation model is developed under various operating conditions using the Matlab/Simulink software (2016b version). Finally, the performance after operation proves that the suggested UPFC with ALTS-PFPNN strategy is installed in multi energy hybrid power grid, which can effectively suppress the severe transient oscillation phenomenon caused by faults in offshore wind farms and wave power farms, and also increase the dynamic phenomenon caused by the randomness of clean energy sources in the overall power grid.

Main innovations and contributions of this paper:

(1) In this paper, the composite multi-energy power system is more in line with the actual power system model and more complex. Adding UPFC can increase the transient stability of the actual grid.
(2) UPFC is a powerful FATCS device. In order to increase the robustness of UPFC, an intelligent control algorithm is proposed.

(3) The system generates the PID correction parameter signal to the UPFC, so that UPFC can produce best damping control for the hybrid power system and achieve a good dynamic response. The proposed algorithm has better control performance than designed PID.

2. System Configuration and Models

2.1. Configuration of the System

Figure 1 is the composite power system diagram studied in this paper. Its renewable energy field includes 4 × 50 MW DFIG based offshore wind farms and three 3 × 40 MW SCIG based sea wave farms are connected to the large power grid through their respective high-voltage AC transmission lines. The proposed UPFC is installed between the PCC coupling bus (Bus 4) and the synchronous generator bus (Bus 6). The studied system's 12 Bus includes battery energy storage system (BESS), synchronous generator (SG), the transformer, the transmission lines, and the infinite bus. All parameters of HPS are displayed in Appendix A.

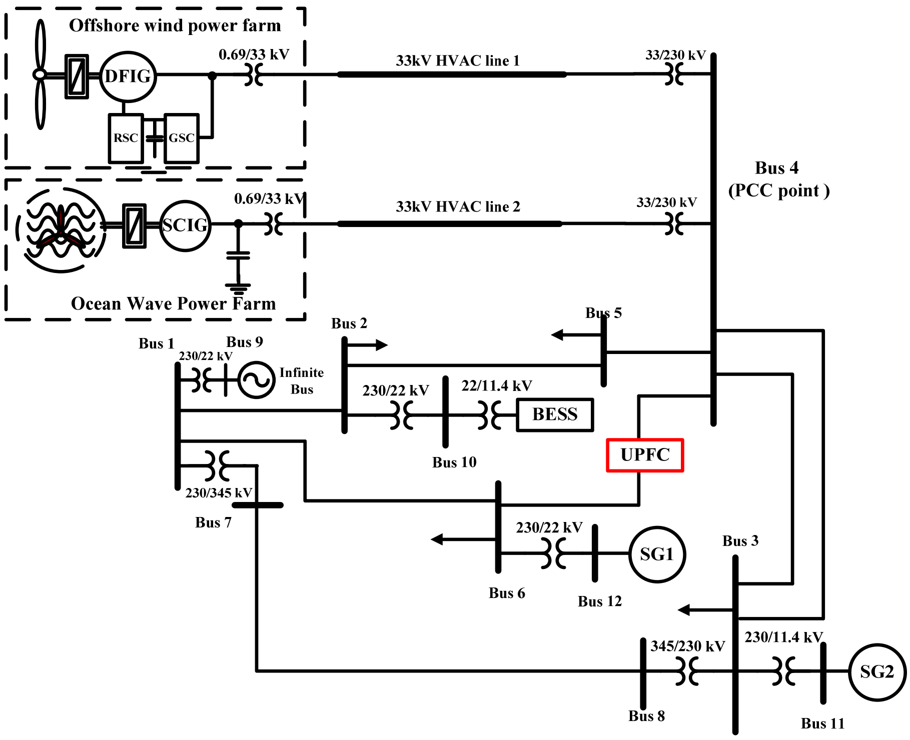

Figure 1. Power grid configuration diagram based on multi energy including UPFC.

2.2. SCIG-Based Wells Turbine Model

The rotating power mechanical torque (T_t) of pneumatic transmission captured from ocean waves as Equation (1). The dimensionless coefficient equation of torque (C_t) is shown in Equation (2). torque coefficient. And incidence angle of air pressure flowing through turbine blades (δ) captured from wave energy can be depicted as [14,15]

$$T_t = kC_t\left(V_A^2 + V_B^2\right), \tag{1}$$

$$C_t = C_8 + \frac{C_1\alpha^3 - C_2\alpha^2 + C_3\alpha - C_4}{C_5\alpha^2 + C_6\alpha - C_7}, \tag{2}$$

$$\alpha = \tan^{-1}\left(\frac{V_A}{V_B}\right), \tag{3}$$

where k is the turbine coefficient, generally taken as 0.5~0.7, V_A is the axial speed of turbine rotor outlet, V_B is the linear speed of blade tip when turbine blade rotates, and C_1–C_8 are constant.

2.3. DFIG-Based Wind Turbine Model

For wind turbines, the input is the wind speed, and the output is the mechanical power that drives the generator rotor to convert electrical energy [2,16]. The mechanical power output (P_m) of the fan blade supplied to the impeller by the wind through the shaft is

$$P_m = \frac{1}{2}\rho A C_p(\lambda, \beta) V_\omega^3 \tag{4}$$

where A is wind energy area swept by acceptable blade rotation of wind turbine, ρ is air density of wind farm, V_ω is air flow velocity of wind, and C_p is the available power coefficient of wind energy of impeller.

2.4. UPFC Model

The topology of UPFC is a integration of a series compensation converter and a shut converter. Its structure is shown in Figure 2, and it includes DC interface capacitor C_{dc}, series and parallel VSC control and parallel and series coupling transformers (T_{sh} and T_{se}), while the leakage inductance of T_{sh} and filter inductance synthesize equivalent inductance L_{sh} and are connected in series with equivalent resistance R_{sh}, while T_{se} The leakage inductance and the filter inductance synthesize the equivalent inductance L_{se} and connect it in series with the equivalent resistance R_{se}.

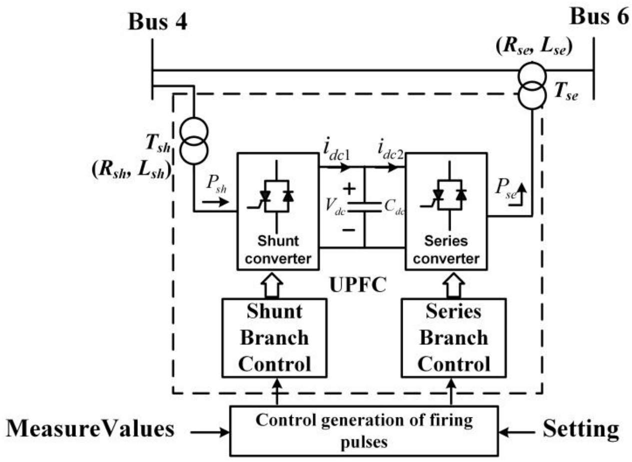

Figure 2. UPFC architecture model connected between Bus 4 and Bus 6.

The UPFC is the most diversified and powerful series-parallel controller in FACTS family. Its structure is shown in Figure 3. UPFC is a combined device that the parallel reactive power compensation part and the series line compensation part are coupled together by a conventional DC link capacitor. It can meanwhile adjust the bus voltage by using shunt branch, and use the series branch controlled power flow [17,18]. It combines the control functions of series equipment and parallel equipment. The shunt terminal voltage source converter functions like a STATCOM, which adjusts the bus voltage by the reactive power sent to the bus. The function of the series terminal voltage source converter is similar to an SSSC, which is equivalent to the impedance of the transmission line by the voltage inserted into the grid via a series compensation converter, the transmission power of the transmission line is adjusted by changing the equivalent impedance parameter of the grid, and bus voltage is stabilized by the parallel converter to stifle power oscillation and improve the stability of the power network.

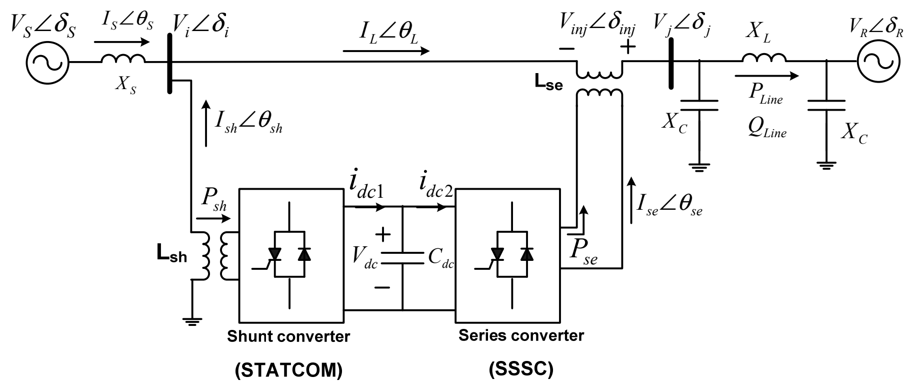

Figure 3. Architecture of UPFC.

3. Design of a Damping Controller for UPFC

The configuration of the proposed ALTS-PFPNN is obtained by using the online learning and training algorithm. The ALTS-PFPNN generate the gains (ΔK_P, ΔK_I and ΔK_D) of PID controller. The control block of the PID controller of the UPFC is shown in Figure 4.

3.1. PID Damping Controller

In this paper, the root locus is used to decide the variables to upgrade the steadiness of the HPS, after linearizing the nonlinear systematic equation at a specific operating point, the matrix of a set of linear system equations is obtained as [19,20]:

$$\dot{X} = AX + BU, \tag{5}$$

$$Y = CX + DU, \tag{6}$$

$$H(s) = Y(s)/U(s) \tag{7}$$

where X and Y are the system state and output matrices respectively, and damping signal $Y = \Delta P_{dam}$. A, B, C and D are coefficient matrices of the relationship between these variable matrices, $X = [X_{DFIG}, X_{SCIG}, X_{TS}, X_{HVDC}, X_{UPFC}]^T$, where X_{DFIG} is state vector of the DFIG, X_{SCIG} is state vector of the SCIG, X_{TS} is state vector of the transmission line and transformer, X_{HVDC} is state vector of the HVDC, X_{UPFC} is state vector of the UPFC, and U is input vector $\Delta\omega_{MS}$.

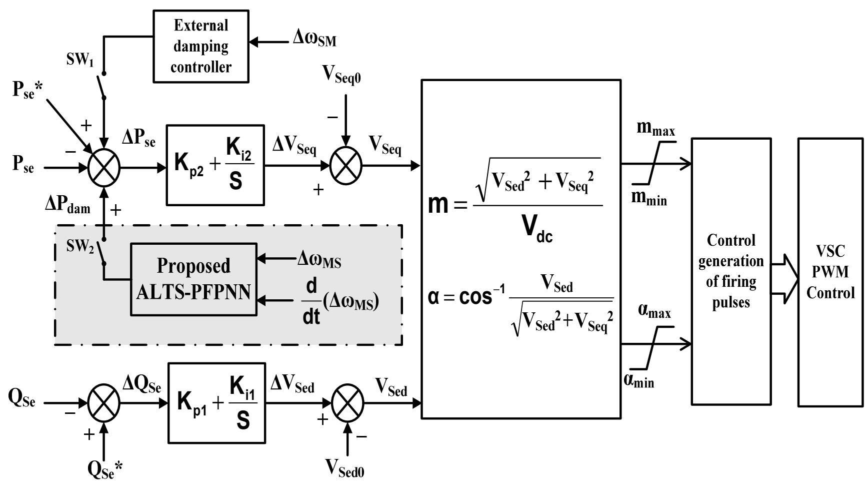

Figure 4. Block Diagram of PID Controller.

3.2. Adaptive Least Trimmed Squares Petri Fuzzy Probabilistic Neural Network (ALTS-PFPNN)

The ALTS-PFPNN control can be processed in parallel and handle uncertainty efficiently. Moreover, the input and output relationship of each layer of ALTS-PFPNN and the mathematical equation of the network learning process are presented. The neuron layer of ALTS-PFPNN has six layers, with two input signals and three output control parameters. Figure 5 is the block diagram of ALTS-PFPNN adjusting control parameters. The basic function of all neuronal layers are introduced as [21–23]. From Figure 5, T_m is the time constant. K_P, K_I, and K_D are the proportional, integral and differential gains of PID controllers. The ALTS-PFPNN produce the variation gains values (ΔK_P, ΔK_I and ΔK_D) of PID controller. K_{Pn}, K_{In}, and K_{Dn} are the updated gains. $\Delta P_{dam,max}$ and $\Delta P_{dam,min}$ is the upper and lower limit of P_{dam}.

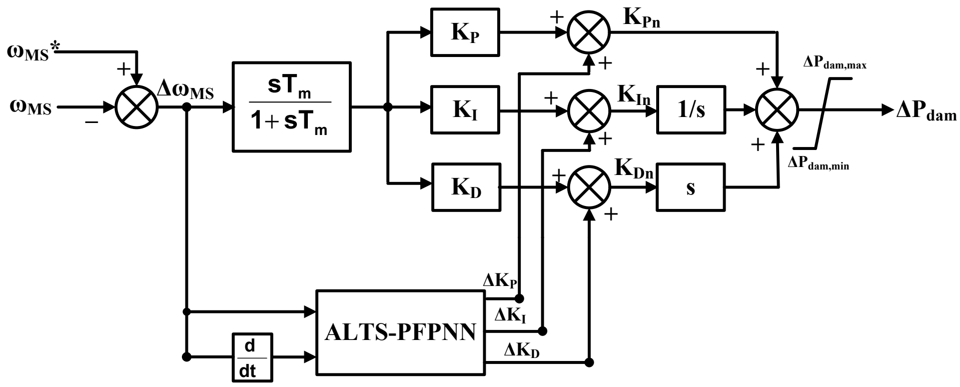

Figure 5. The structure of an ALTS-PFPNN.

3.2.1. ALTS-PFPNN Structure

The input signal of ALTS-PFPNN is only used for signal propagation, so in the first layer, it is only necessary to propagate the input information x_i of the ith neuron iteration Nth to the output of the neuron in this layer, as shown in Equation (8). This input element is the tracking error e_{qk} between the reference value ω^*_{MS} and the actual value ω_{MS} of the rotor velocity and the differential term of this error $\dot{e}_{qk}$. The output value of the first layer is propagated to the Gaussian function of the second layer neuron for activation $\mu_j(x_i)$, as shown in Equation (9).

$$x_i(N) = e_i(N) i = 1,2 \tag{8}$$

$$\mu_j(x_i) = \exp(net_j^2(N)) = \exp\left(-\frac{(x_i(N) - c_j)^2}{v_j^2}\right), \quad j = 1,2,\ldots,6 \tag{9}$$

where c_j and v_j denote the center and base of Gaussian function of the second layer neuron.

The transition value T_p is fired or unfired in the third layer and its threshold value D_{th} are expressed as Equations (10) and (11). The input and output information of this layer of Petri neurons are as follows Equations (12) and (13).

$$T_p(N) = \begin{cases} 1, & \mu_j(N) \geq D_{th} \\ 0, & \mu_j(N) < D_{th} \end{cases}, \quad th = 1,2,\ldots,6 \tag{10}$$

$$D_{th} = \frac{\delta \exp(-\gamma V)}{1 + \exp(-\gamma V)} \tag{11}$$

$$net_p(N) = \begin{cases} \mu_j(N)\ , & T_p(N) = 1 \\ 0\ , & T_p(N) = 0 \end{cases} \tag{12}$$

$$\mu_p(N) = f_p(net_p(N)) = net_p(N),\ p = 1,2,\ldots,6 \tag{13}$$

where V is the average value $(e_{qk} + \dot{e}_{qk})^{-1}$ of the input variable of ALTS-PFPNN. δ and γ are positive coefficients of the threshold parameter.

After entering the probability layer from the Petri layer, the output $P_k(\mu_p)$ is activated by the neurons of the inverted bell-Gaussian function. The weights of this layer are the c_k and ν_k of the center and base of the Gaussian function. The activated signals P_l^I of the fourth layer and the output signals μ_l^I of the second layer are used as the input signals of the fifth layer neurons to establish the fuzzy rule base μ_l^O. The weight value w_{ji} of the second to fifth layers is an important training parameter, and the weight value w_{kl} of the fourth to fifth layers is also an important training parameter. The signals of these layers are transmitted to the sixth layer for integration to obtain the output signals $y(N)$ of the controller. The output signals ΔK_P, ΔK_I and ΔK_D in ALTS-PFPNN are the adjustment signals to the parameters of the PID controller. The weight w_l of the sixth layer is also one of the training parameters. The input and output relations of the above layers are as follows:

$$P_k(\mu_p) = \exp\left(-\frac{(\mu_p - c_k)^2}{v_k^2}\right),\ k = 1, 2, \ldots, 18 \tag{14}$$

$$\mu_l^I = \prod_j w_{jl}\mu_j \tag{15}$$

$$P_l^I = \prod_k w_{kl}P_k \tag{16}$$

$$\mu_l^O = \mu_l^I P_l^I,\ l = 1, 2, \ldots, 9 \tag{17}$$

$$y(N) = \sum_{l=1}^{9} w_l \mu_l^O \tag{18}$$

3.2.2. Online Learning and Training Process

So as to introduce the learning algorithms of the proposed ALTS-PFPNN using incremental gradient descent algorithm, the adaptive least trimmed squared errors defined as [24,25]:

$$e_{qk} = (\omega_{MS}^* - \omega_{MS}) \tag{19}$$

$$E = \frac{1}{2}\sum_{q=1}^{l} \alpha_{R(e_{qk}^2)} e_{qk}^2 \tag{20}$$

The trimming percentage α can be defined as

$$\alpha = ((l - h)/l) \times 100\% \tag{21}$$

where α is set as a constant. The penalizing weight $\alpha_{R(e_{qk}^2)}$ can be written as

$$\alpha_{R(e_{qk}^2)} = \begin{cases} 1, & 1 \le R(e_{qk}^2) \le h \\ 0, & h < R(e_{qk}^2) \le l \end{cases} \tag{22}$$

The best robustness properties are achieved when $h = l/2$, $R(e_{qk}^2)$ denotes the rank of the residual e_{qk}^2 among $e_{1k}^2, \ldots, e_{lk}^2$ and $e_{(1)k}^2 \le \ldots \le e_{(l)k}^2$ are the ordered values of $e_{1k}^2, \ldots, e_{lk}^2$ [24].

The weight training of ALTS-PFPNN is a learning algorithm using the Back Propagation (BP) network developed on the basis of the δ rule. The error term backpropagated from the output layer, the subscript symbols (o, l, j) of δ and weight adjustment amount $\Delta\omega$ represent layers 6, 5 and 2 respectively.

$$\delta_0 = -\frac{\partial E}{\partial y(N)} = -\frac{\partial E}{\partial \omega_{MS}}\frac{\partial \omega_{MS}}{\partial y(N)} \tag{23}$$

$$\Delta w_l = -\eta_1 \frac{\partial E}{\partial y(N)} \frac{\partial y(N)}{\partial w_l} = \eta_1 \delta_0 \mu_l^O \tag{24}$$

$$\delta_l = -\frac{\partial E}{\partial \mu_l^O} = -\frac{\partial E}{\partial y(N)} \frac{\partial y(N)}{\partial \mu_l^O} = \delta_0 w_l \tag{25}$$

$$\delta_j = -\frac{\partial E}{\partial \mu_j} = -\frac{\partial E}{\partial y(N)} \frac{\partial y(N)}{\partial \mu_l^O} \frac{\partial \mu_l^O}{\partial \mu_l^I} \frac{\partial \mu_l^I}{\partial \mu_j} = \sum_l \delta_l P_l^I \tag{26}$$

Similarly, the weights correction amount of Gaussian function are Δc_j and $\Delta \nu_j$ respectively, so the weights correction amount and the weights adjustment formula are described as follows:

$$\begin{aligned} \Delta c_j = -\eta_2 \tfrac{\partial E}{\partial c_j} &= -\eta_2 \tfrac{\partial E}{\partial y(N)} \tfrac{\partial y(N)}{\partial \mu_l^O} \tfrac{\partial \mu_l^O}{\partial \mu_l^I} \tfrac{\partial \mu_l^I}{\partial \mu_j} \tfrac{\partial \mu_j}{\partial net_j^2} \tfrac{\partial net_j^2}{\partial m_j} \\ &= \eta_2 \delta_j \tfrac{2(x_i - c_j)}{v_j^2} \end{aligned} \tag{27}$$

$$\begin{aligned} \Delta v_j = -\eta_3 \tfrac{\partial E}{\partial v_j} &= -\eta_3 \tfrac{\partial E}{\partial y(N)} \tfrac{\partial y(N)}{\partial \mu_l^O} \tfrac{\partial \mu_l^O}{\partial \mu_l^I} \tfrac{\partial \mu_l^I}{\partial \mu_j} \tfrac{\partial \mu_j}{\partial net_j^2} \tfrac{\partial net_j^2}{\partial \sigma_j} \\ &= \eta_3 \delta_j \tfrac{2(x_i - c_j)^2}{v_j^3} \end{aligned} \tag{28}$$

$$c_j(N+1) = c_j(N) + \Delta c_j \tag{29}$$

$$v_j(N+1) = v_j(N) + \Delta v_j \tag{30}$$

$$w_l(N+1) = w_l(N) + \Delta w_l \tag{31}$$

where η is the learning rate of their own weights.

4. Simulations and Discussion

This section mainly tests the effectiveness of the designed UPFC and damping controller for power flow control and stability improvement of the wind-wave power generation systems with different operating conditions [26–32]. The performance of the ALTS-PFPNN is compared to the designed PID controllers. These methods are investigated through cases simulation tests. The property of each scheme as shown in Figures 6–8 and aggregated in Tables 1 and 2.

4.1. Random Variable Velocity for Wind and Wells Turbine

Figure 6 demonstrates the comparative transient response of the research system during wind and wave speed change. Simulate the dynamic response between 0 s to 46 s, in which the wave speed varies randomly from 0 s to 22 s. We simulates actual ocean disturbances in 3 s, 7.5 s, 11.5 s, 16 s and 21 s, and the wind speed varies randomly in 24 s to 46 s. Figure 6a,b obvious the active and reactive power response of the offshore wind power farm, respectively. Disturbance change of reactive power due to change of active power. If UPFC is used, the amplitude of active and reactive power in offshore wind farms can be decreased. If proposed damping controller is combined with UPFC, it can effectively realize the minimum amplitude of active and reactive power in wind farms. Active and reactive power responses of the ocean wave farm are similar to those shown in Figure 6c,d, respectively.

If UPFC is used, the bus voltage is increased through the reactive power of UPFC are shown in the Figure 6e,f. The figures show the voltage magnitude responses for Bus 4 and Bus 6, respectively. From the Figure 6e,f, during the wind and wave speed variety, the voltage levels of Bus 4 and Bus 6 will also be influenced. The proposed damping controller is used in combination with UPFC, the voltage amplitudes of two buses should be minimal changes. Figure 6g depicts the reactive power response of UPFC. It is obvious that when the voltage rise changes, UPFC can generate reactive power to stabilize the voltage and also support bus voltage.

4.2. Ultra-Short Time Three Phase Short Circuit Fault at Bus (0.1 s)

Simulate the three phase short circuit fault on Bus 4 at 1 s, the fault time is continued for 0.1 s, and the changes of each parameter are observed. Figure 7 illustrates the transient response of the investigated integrated system during three phase short circuit fault occurs at Bus 4. Figure 7a,b represents the transient response of active power in the offshore wind power farm and active power in the ocean wave power farm, respectively. Compared with the damping controllers of Designed PID, the UPFC of ALTS-PFPNN has the best oscillation suppression effect. The steady-state can be restored in about 2.3 s, and it is found that ALTS-PFPNN also has the smallest excess. From the Figure 7c,d, the reactive power compensated by UPFC controlled by ALTS-PFPNN can make the Bus 4 voltage of SG1 rise and return to stability quickly, and also keep the voltage of Bus 6 at 1 pu. Without UPFC compensation, the Bus 4 voltage cannot be increased, which also causes continuous voltage oscillation until 4.9 s, but the voltage of bus 6 has dropped below 1 pu. When the fault occurs, the rotor speeds of SG1 and SG2 in the grid oscillate violently are shown in Figure 7e,f. When there is UPFC, the rotor speed can come back to the stable as soon as possible, while it will oscillate continuously for a period of time when there is no UPFC. Figure 7g shows the rotor angle deviation between SG1 and SG2. The results show that UPFC with ALTS-PFPNN control can make the angle deviation return to the steady state as quickly as possible, while without UPFC returns to the steady state as slowly as possible, followed by designed PID controller. Due to the large amplitude oscillation change of bus voltage caused by the fault, UPFC provides a large amount of reactive power to stabilize the bus voltage. The response of maintained voltage is shown in Figure 7h. As seen from the above results, the UPFC with advanced ALTS-PFPNN method can maintain the system in a good transient response, and its effect is better than other controllers.

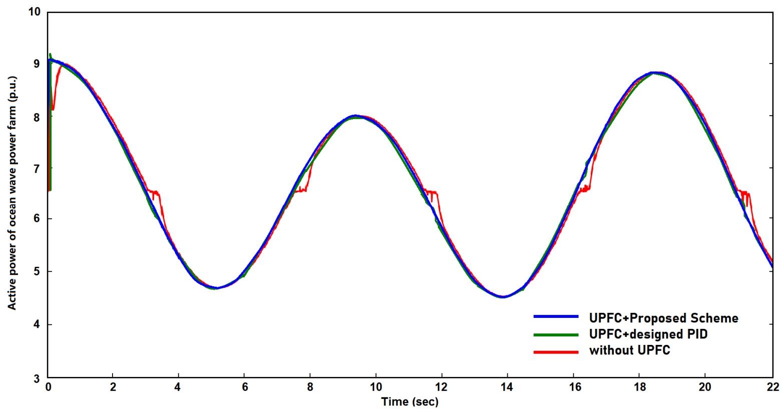

(**a**)

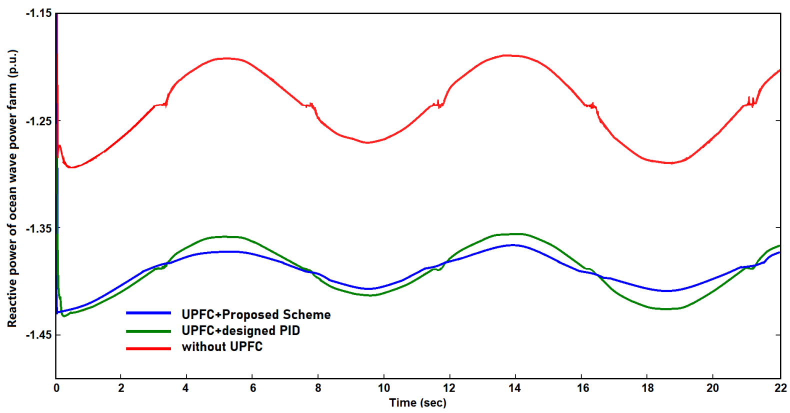

(**b**)

Figure 6. *Cont.*

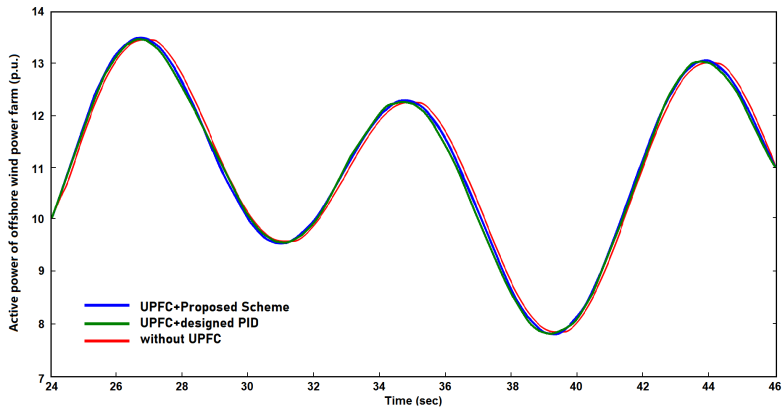

(c)

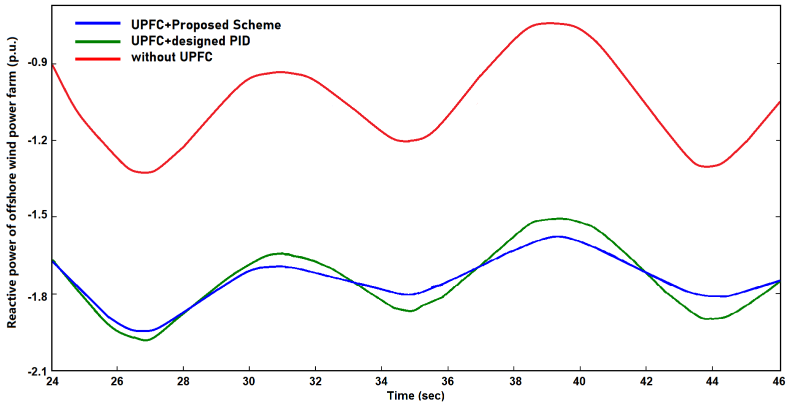

(d)

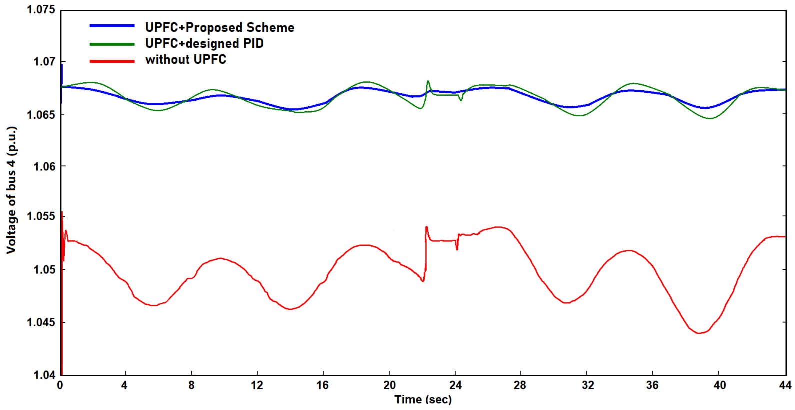

(e)

Figure 6. *Cont.*

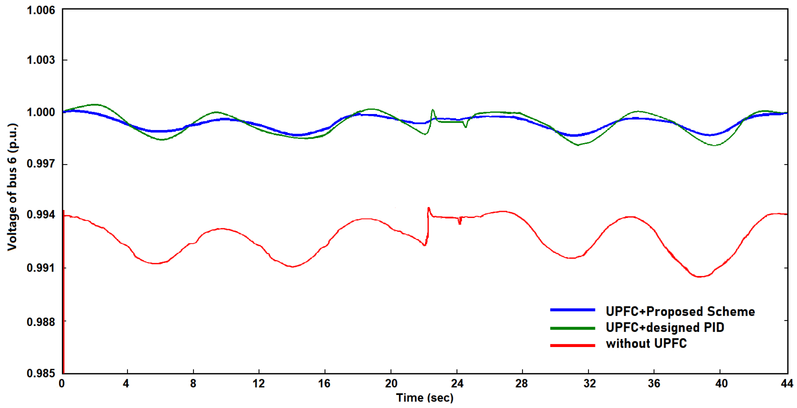

(**f**)

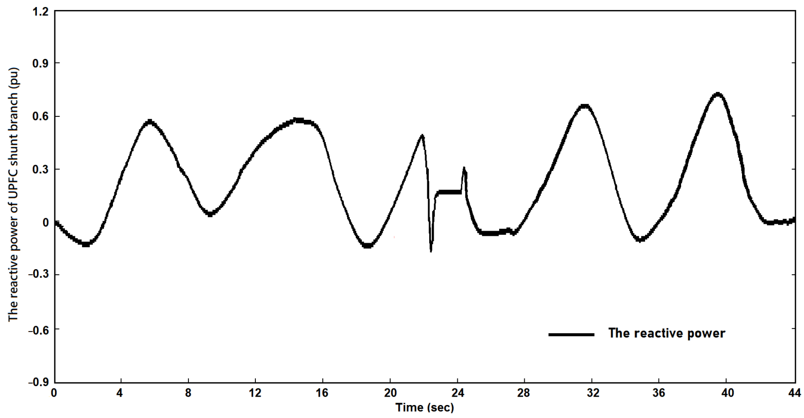

(**g**)

Figure 6. Transient responses of the proposed system with wind and wave speed changes: (**a**) Active power response of Line 2, (**b**) Reactive power response of Line 2, (**c**) Active power response of Line 1, (**d**) Reactive power response of Line 1, (**e**) Voltage of Bus 4, (**f**) Voltage of Bus 6, (**g**) Reactive power response of UPFC.

4.3. Short Time Three Phase Short Circuit Fault at Bus (0.5 s)

Simulate the three phase short circuit fault on Bus 4 at 1 s, the fault time is maintained for 0.5 s, and the changes of each parameter are observed. The fault time is too long and the renewable energy that is not added to the UPFC in the power grid is urgently removed. It can be clearly observed from the transient responses shown in Figure 8 that the HPS without UPFC is unstable fluctuations. Figure 8a,b represent the transient responses of the active power of wind and ocean wave power farm, respectively. Compared with the damping controllers of Designed PID, the UPFC of ALTS-PFPNN has the best oscillation suppression effect. The steady-state can be restored in about 8.5 s, and it is found that ALTS-PFPNN also has the smallest excess. From Figure 8c,d that the reactive power compensated by UPFC controlled by ALTS-PFPNN can make the voltage of bus 4 of SG1 rise rapidly and restore stability, and can also keep the voltage of bus 6 at 1 pu. As can be seen from the figure that the UPFC with ALTS-PFPNN can maintain the bus voltage at the minimum voltage change, while the system voltage without UPFC will not be able to maintain the target value. When the fault occurs, the rotor speed of SG1 and SG2 in the power grid oscillates violently, as shown in Figure 8e,f. When there is UPFC, the rotor speed can be restored to stable as soon as possible, while without UPFC, the generator is out of control and cannot converge. Figure 8g shows the rotor angle deviation between SG1 and SG2. The same results show that UPFC with ALTS-PFPNN control can make the angle deviation recover to the steady-state as soon as possible, and then the PID controller is designed to recover to the steady-state slowly, while UPFC without UPFC cannot converge. As the bus voltage oscillates greatly due to the fault, UPFC provides a lot of reactive power to stabilize the bus voltage. The maintenance voltage response is shown in Figure 7h. Compared with Designed PID and ALTS-PFPNN in the UPFC proposed in this paper is the most effective to reduce the oscillation of the bus voltage after the fault and increase the transient stability.

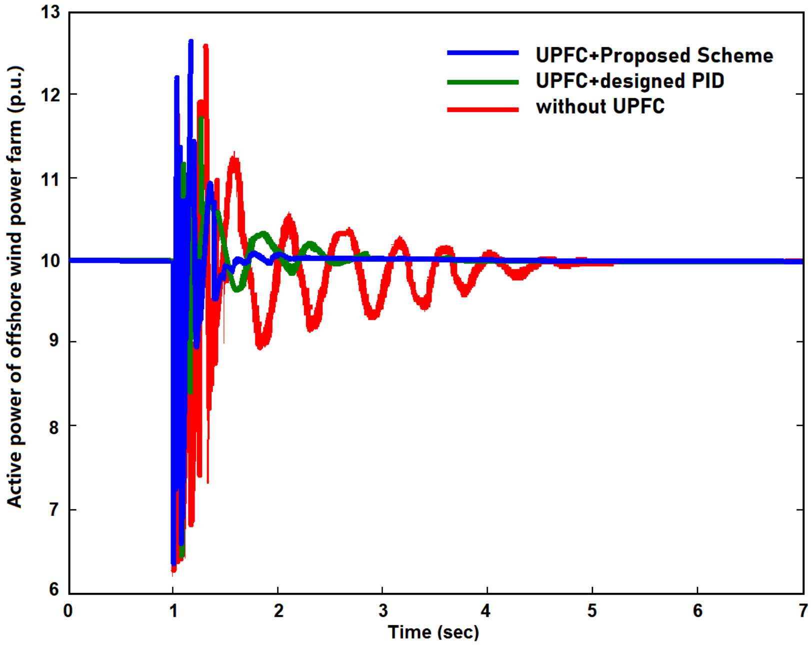

(**a**)

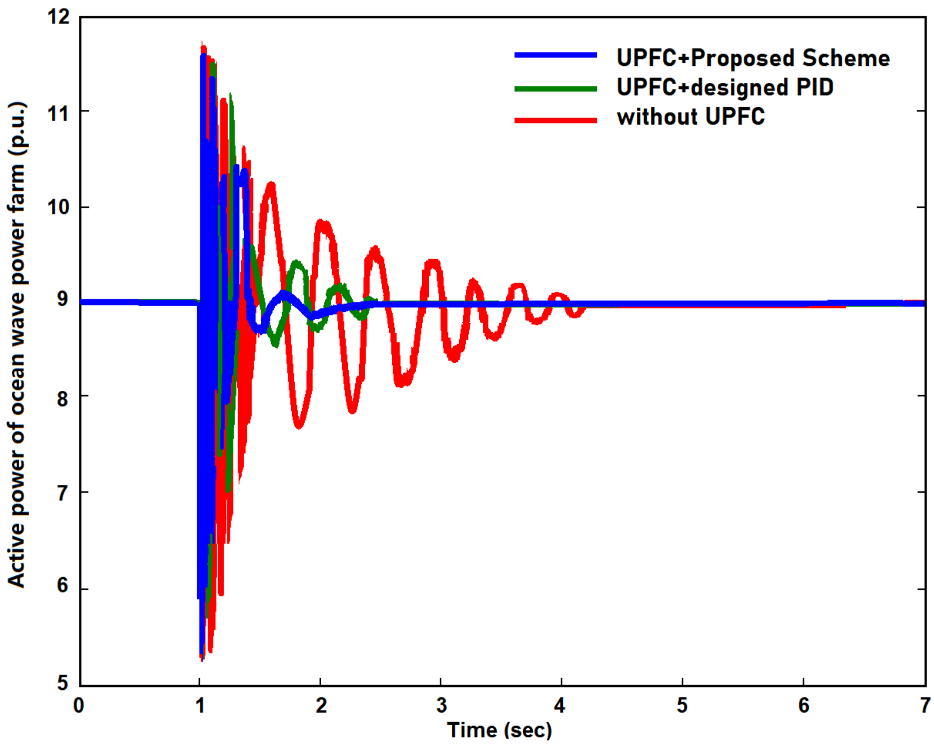

(**b**)

Figure 7. *Cont.*

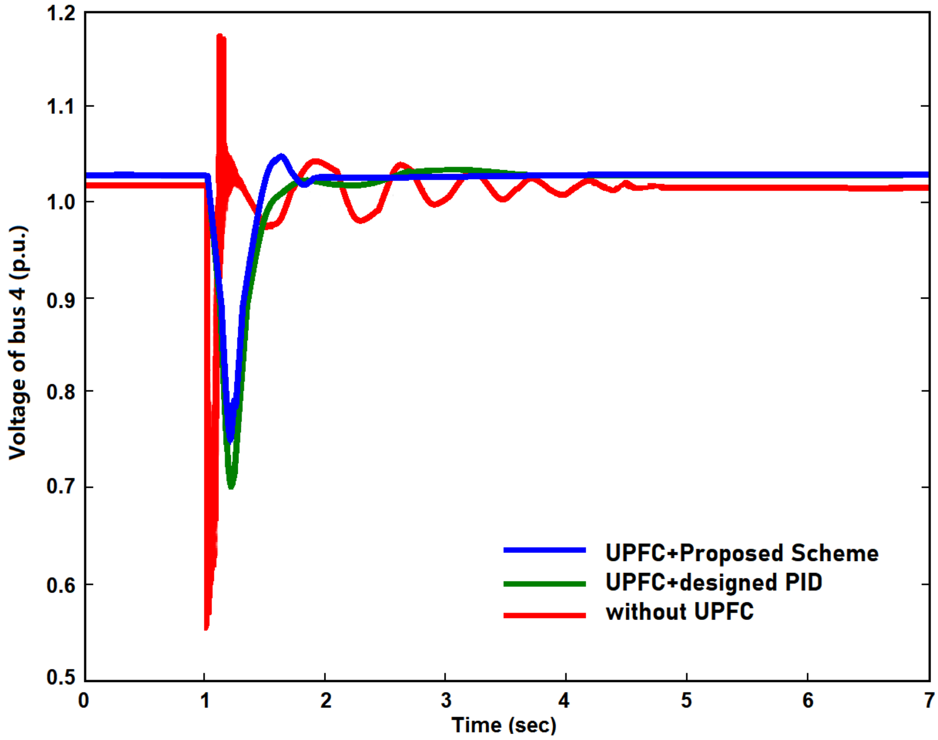

(c)

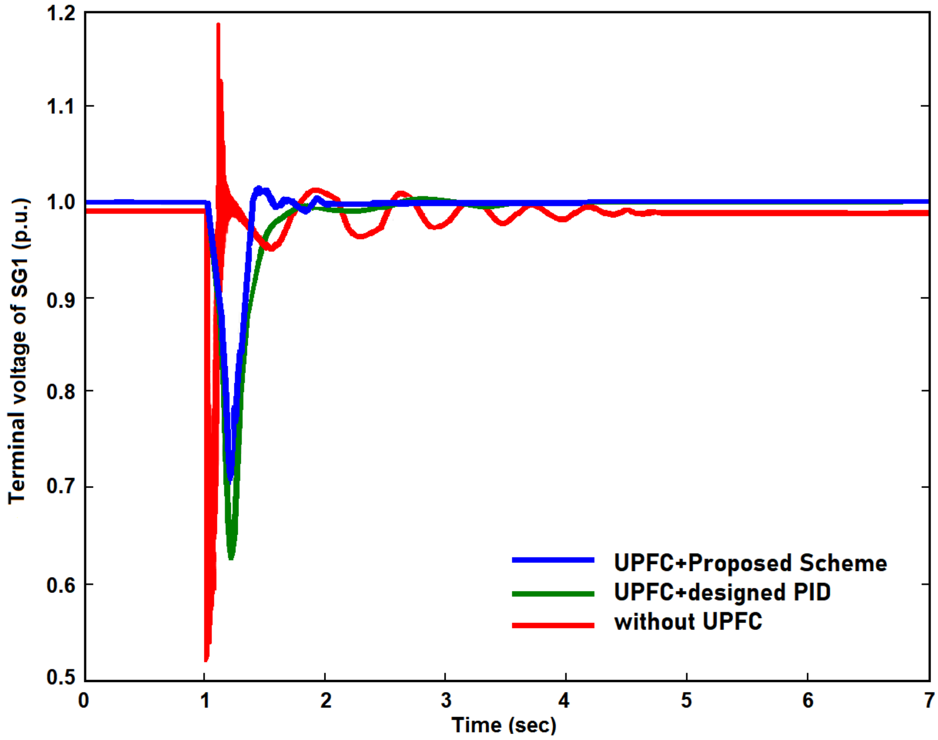

(d)

Figure 7. *Cont.*

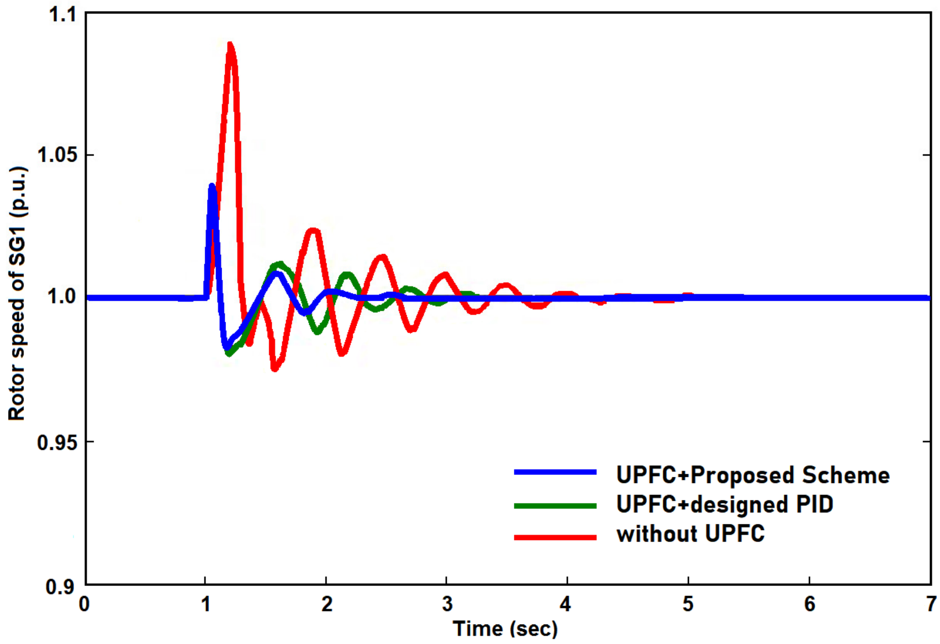

(**e**)

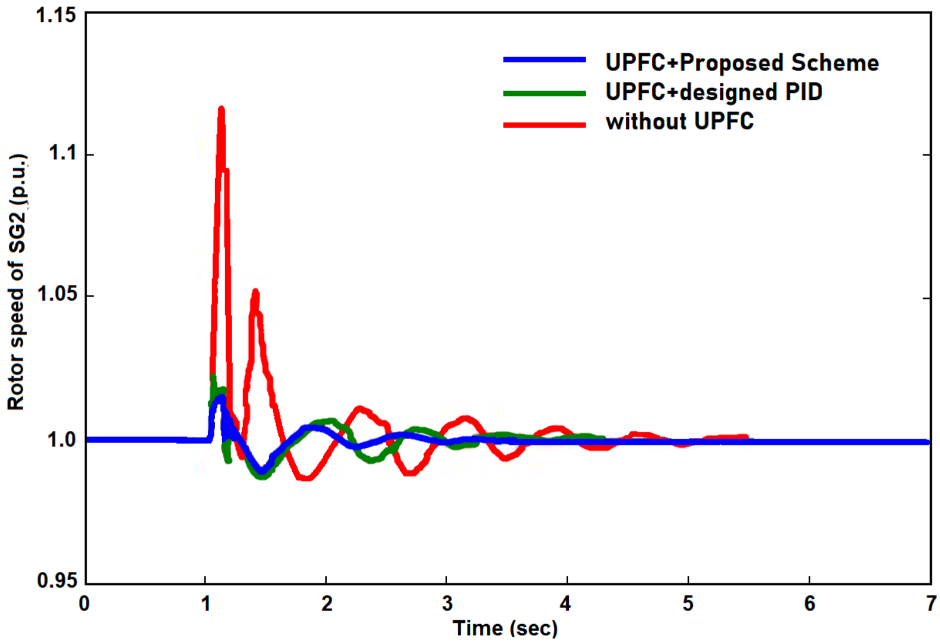

(**f**)

Figure 7. *Cont.*

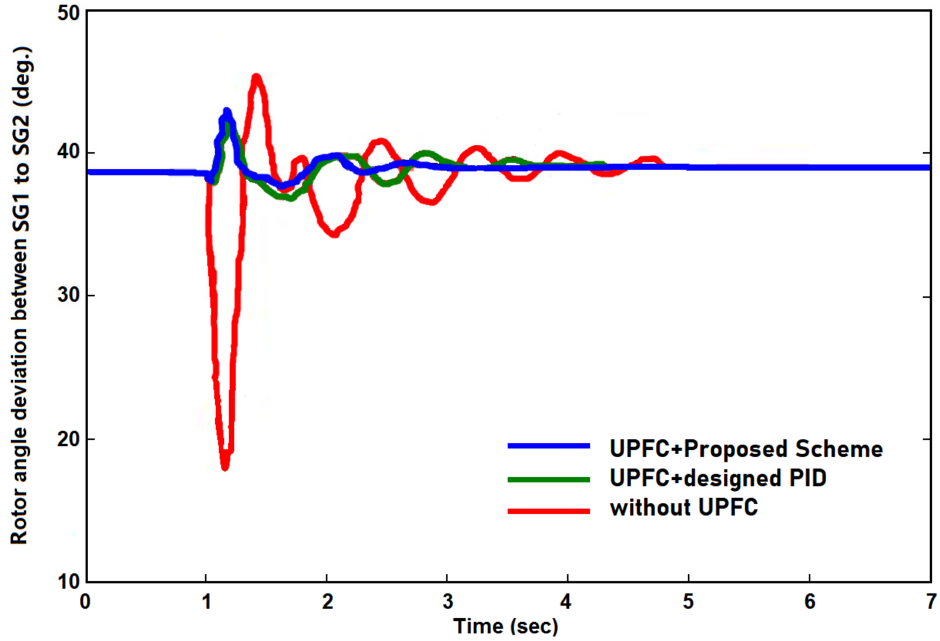

(g)

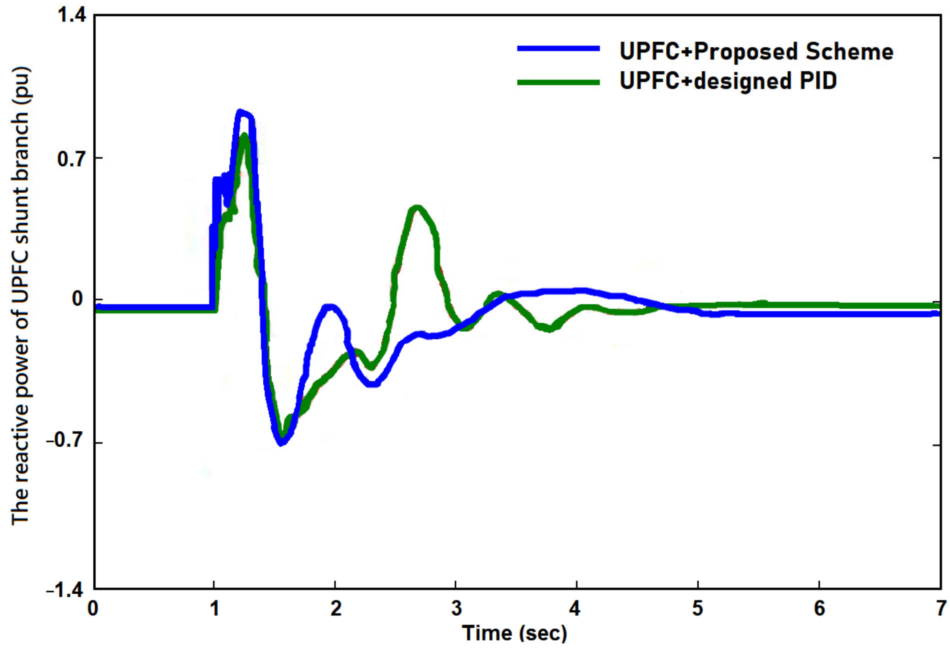

(h)

Figure 7. Transient responses of the proposed system for three phase short circuit fault for 0.1 s at the grid: (**a**) Active power response of Line 1, (**b**) Active power response of Line 2, (**c**) Voltage of Bus 4, (**d**) Terminal voltage of SG1, (**e**) Rotor speed of SG1, (**f**) Rotor speed of SG2, (**g**) Rotor angle deviation between SG1 to SG2, (**h**) Reactive power response of UPFC.

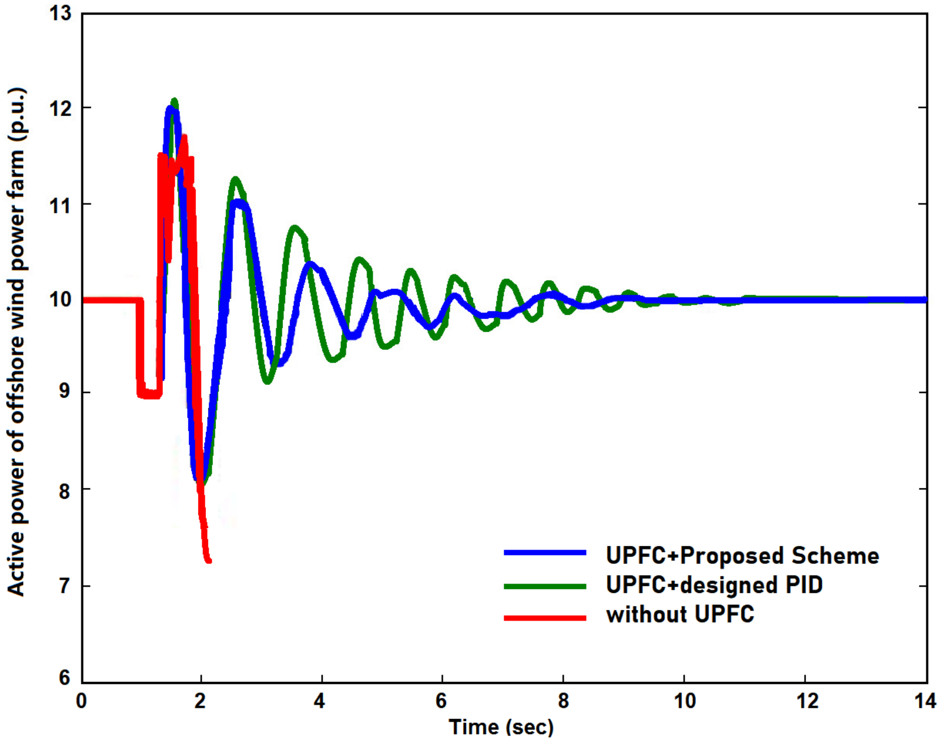

(**a**)

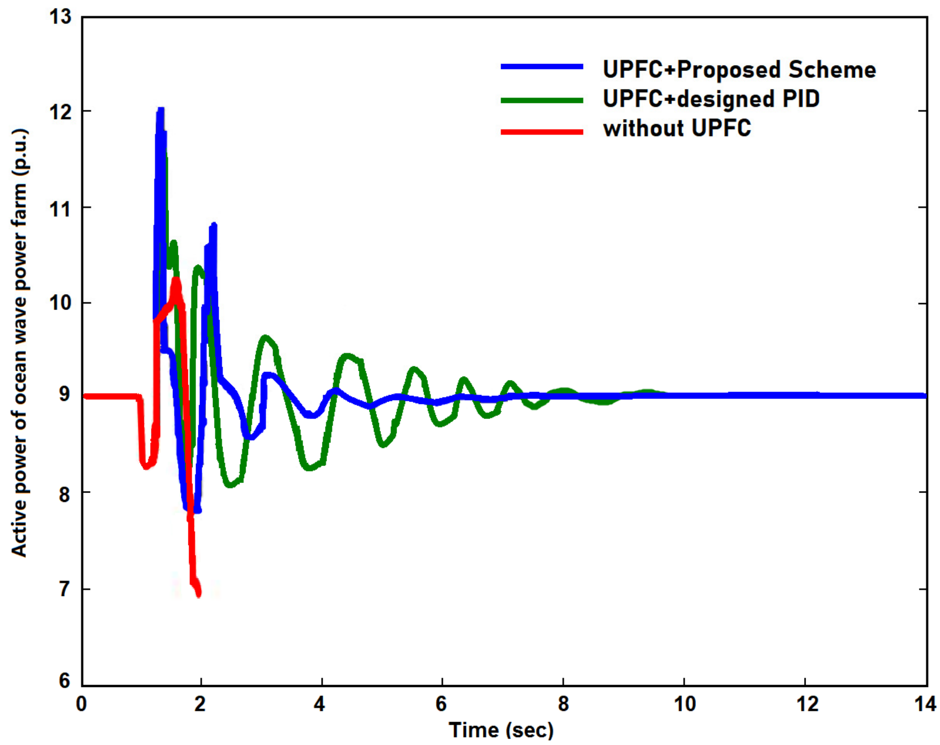

(**b**)

Figure 8. *Cont*.

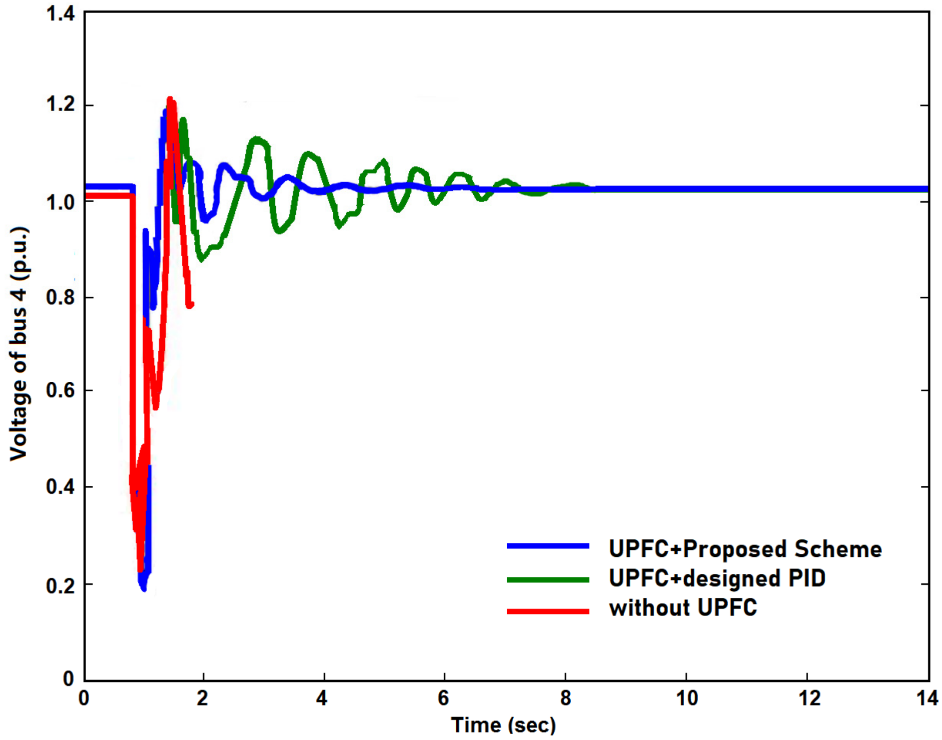

(**c**)

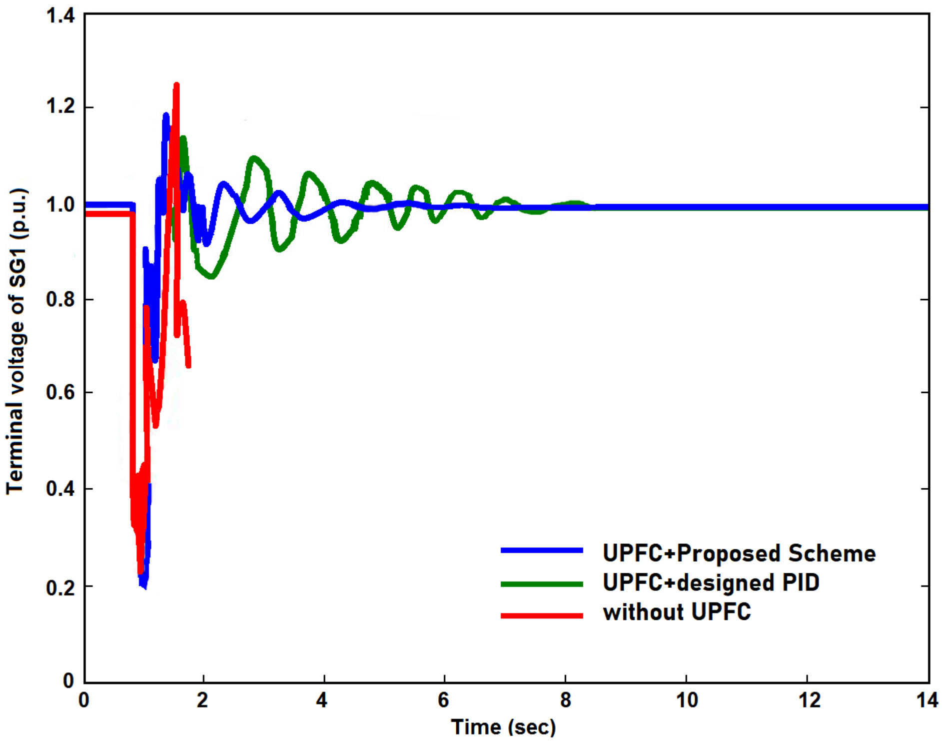

(**d**)

Figure 8. *Cont.*

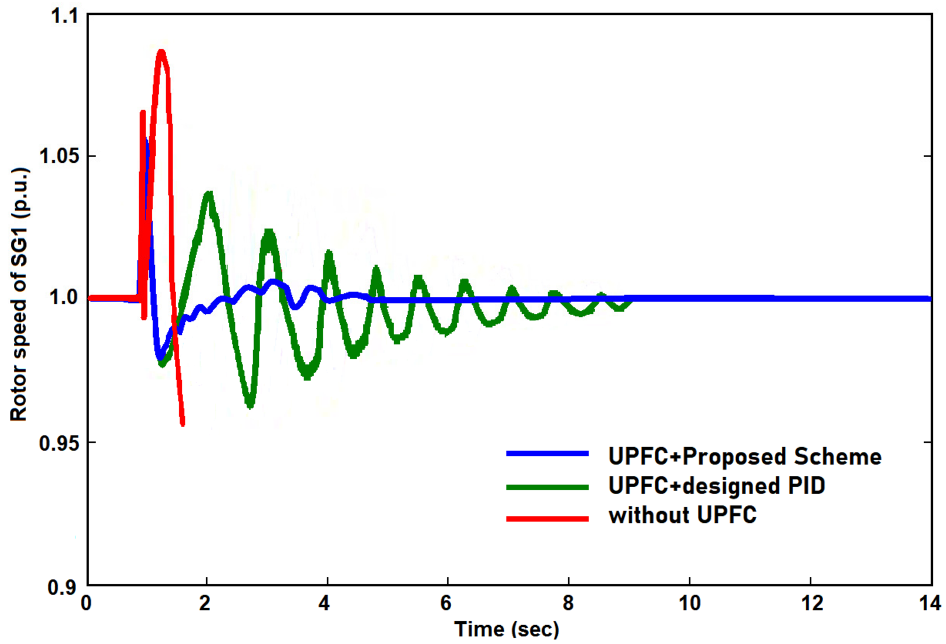

(e)

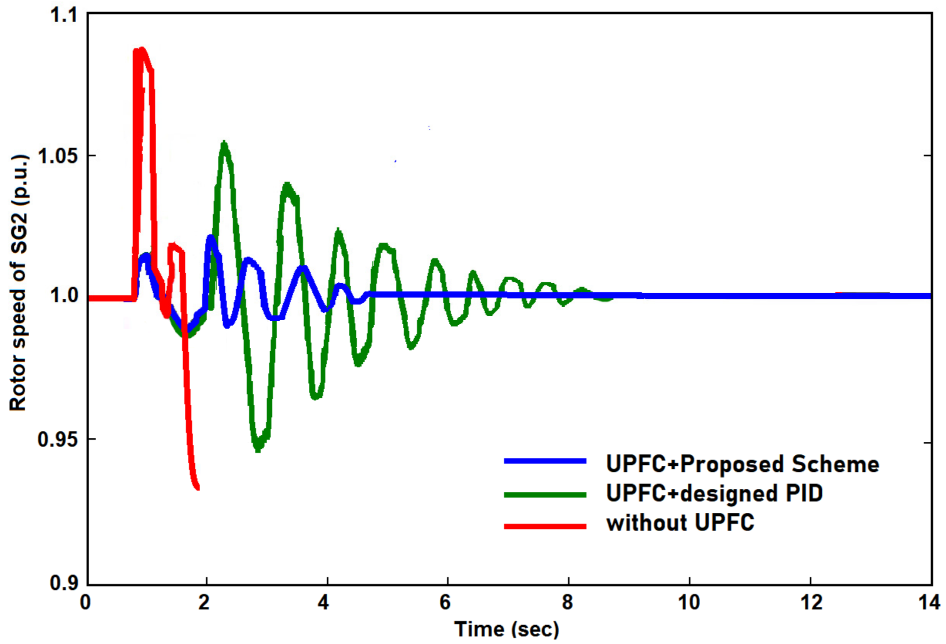

(f)

Figure 8. *Cont.*

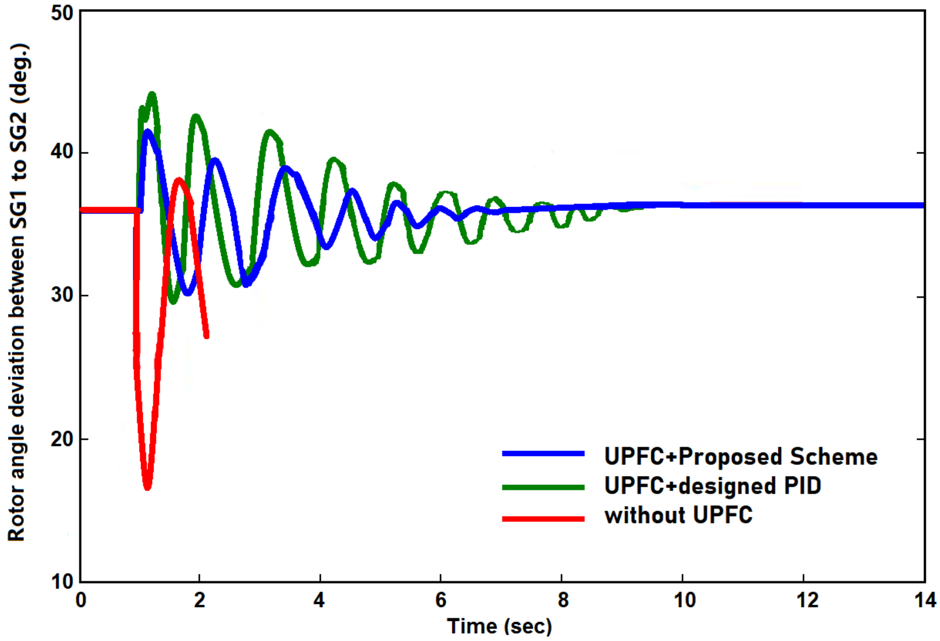

(g)

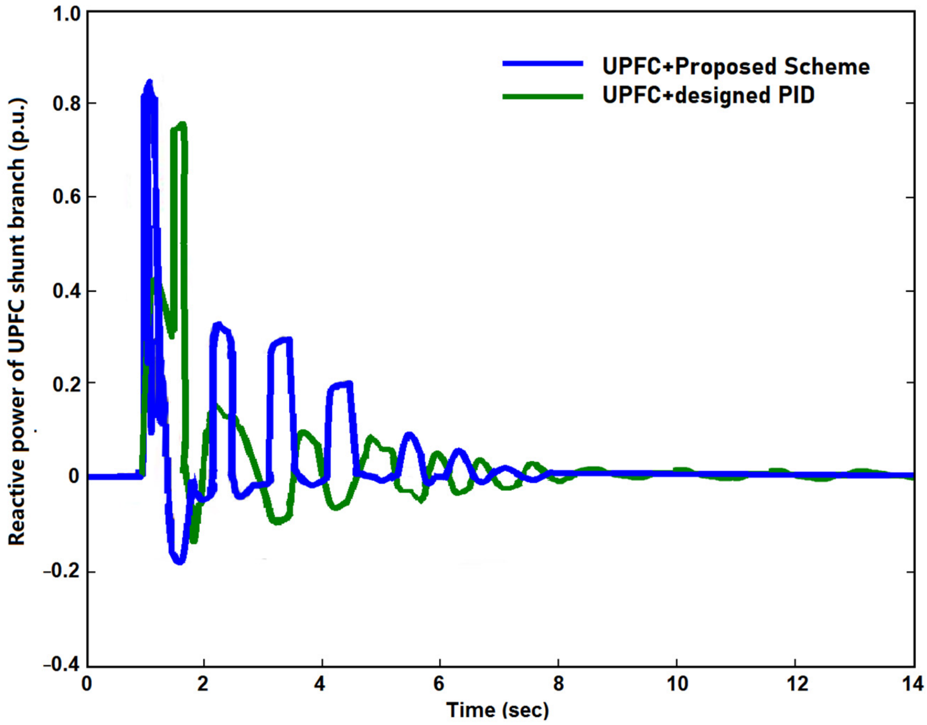

(h)

Figure 8. Transient responses of the proposed system for three phase short circuit fault for 0.5 s at the grid: (**a**) Active power response of Line 1, (**b**) Active power response of Line 2, (**c**) Voltage of Bus 4, (**d**) Terminal voltage of SG1, (**e**) Rotor speed of SG1, (**f**) Rotor speed of SG2, (**g**) Rotor angle deviation between SG1 to SG2, (**h**) Reactive power response of UPFC.

On the other hand, the proposed technique compare with other two methods in Tables 1 and 2, without UPFC, UPFC + designed PID, and UPFC + Proposed Scheme, in terms of system behavior in grid side. It can be observed that the provided UPFC +

Proposed Scheme has a better result on voltage regulation and voltage vibration in terms of load disturbance and three phase short circuit faults.

Table 1. Dynamic performance comparison under load disturbance.

Scheme	Without UPFC (p.u.)	Designed PID (p.u.)	Proposed Scheme (p.u.)
Bus 4 Voltage (avg.)	1.0512	1.0654	1.0655
Bus 6 Voltage (avg.)	0.9927	1.0016	1.0014
Active power of offshore wind farm	10.8934	10.9644	11.1467
Active power of ocean wave farm	5.9754	6.3174	6.7785
Integral absolute error (10^{-6} p.u.)	101.4280	88.6830	84.4710
Max. absolute error (10^{-3} p.u.)	18.8000	4.5800	4.4900

Table 2. Dynamic performance comparison under three phase short circuit fault.

Scheme	Without UPFC (p.u.)	Designed PID (p.u.)	Proposed Scheme (p.u.)
Bus 4 Voltage (avg.)	1.0234	1.0467	1.0561
Bus 6 Voltage (avg.)	0.99457	1.00461	1.0052
Max. Transient Grid-Side Voltage Overshoot	0.2571	0.2571	0.2571
Max. Transient Grid-Side Voltage Undershoot	0.4721	0.3682	0.0957
Integral absolute error (10^{-3} p.u.)	65.4340	12.3959	6.7914
Max. absolute error (p.u.)	2.9430	1.8416	0.9841

5. Conclusions

This paper successfully demonstrates the advanced ALTS-PFPNN scheme in HPS to improve the stability of the grid. The dynamic and transient responses of the system under the change of wind and wave speed and three phase short circuit faults demonstrate the efficiency of the proposed control strategy. With the vigorous development of renewable energy, the proportion of hybrid power generation in the electrical network has gradually increased, and the high proportion and high penetration rate of hybrid power generation will inevitably affect the safely and stable operation in the grid. Therefore, this article provides an intelligent control architecture by integrating the UPFC device of the flexible AC transmission system, so that the power system installed with the offshore wind farm can maintain good dynamic characteristics under various operating conditions, while improving the regeneration of wind power. The system generates PID correction parameter signals ΔK_P, ΔK_I, ΔK_D to UPFC, so that UPFC can produce the best damping control for the hybrid power system, and it can provide better dynamic characteristics and transient stability in a wide working range.

Author Contributions: Methodology, K.-H.L. and C.-M.H.; software, K.-H.L.; writing—original draft preparation, C.-M.H.; formal analysis, C.-M.H.; writing—review and editing, C.-M.H. and K.-H.L.; supervision, F.-S.C.; project administration, F.-S.C. All authors have read and agreed to the published version of the manuscript.

Funding: This research received no external funding.

Institutional Review Board Statement: Not applicable.

Informed Consent Statement: Not applicable.

Data Availability Statement: Data is contained within the article.

Acknowledgments: The project was supported by the Natural Science Foundation of Fujian Province of China (No. 2021J01531).

Conflicts of Interest: The authors declare no conflict of interest.

Appendix A

DFIG-based OWF, SG and transmission line
S_{SG} = 555 MVA , S_{DFIG} = 5 × 20 MW, 3.75 A, 3000 r/min, ρ = 1.25 kg/m³, r = 0.5 m, T_C = 0.69/33 kV, J = 1.32 × 10^{-3} Nms², B = 5.78 × 10^{-3} Nm s/rad, V = 15 KV, PF = 0.975, R_{L1} = R_{L2} = 0 pu, X_{L1} = 0.6 pu, X_{L2} = 0.4 pu, R_{SG} = 0 pu, X_{SG} = 0.0012 pu, f = 60 Hz, T_1 = 15/161 KV, T_2 = 23/161 KV, R_t = 0.001 pu, X_{SG} = 0.0125 pu, R_{L1} = R_{L2} = 0 pu, X_{L1} = X_{L2} = 0.0125 pu, The system contains 200 MW DFIG-based Offshore Wind Power Farm, 120 MW SCIG-based Ocean Wave Power Farm, BESS (128 MW, 11.4 kV), 33 kV HVAC.
UPFC with control system
S_{upfc} = 160 MVA, V = 22 KV, R_{se} = R_{sh} = 0.01 pu, X_{se} = X_{sh} = 0.1 pu, K_1 = 15, K_2 = 15, K_3 = 1, K_{p4} = 0.1, T_1 = 0.15 s, T_2 = 0.1 s, T_3 = 0.5 s, T_4 = 0.2 s

Figure A1. All parameters of HPS.

References

1. Ou, T.C.; Lu, K.H.; Huang, C.J. Improvement of transient stability in a hybrid power multi-system using a designed NIDC. *Energies* **2017**, *10*, 488. [CrossRef]
2. Lu, K.H.; Hong, C.M.; Xu, Q.Q. Recurrent Wavelet-based Elman Neural Network Control for Integrated Offshore Wind and Wave Power Generation Systems. *Energy* **2019**, *170*, 40–52. [CrossRef]
3. Lin, C.J.; Yu, O.S.; Chang, C.L.; Liu, Y.H.; Chuang, Y.F.; Lin, Y.L. Challenges of wind farms connection to future power systems in Taiwan. *Renew. Energy* **2009**, *34*, 1926–1930. [CrossRef]
4. Lin, F.J.; Huang, Y.S.; Tan, K.H.; Lu, Z.H.; Chang, Y.R. Intelligent-controlled doubly fed induction generator system using PFNN. *Neural Comput. Appl.* **2013**, *22*, 1695–1712. [CrossRef]
5. Hart, S.J.; Shaffer, R.E.; Rose-Pehrsson, S.L.; McDonald, J.R. Using physics-based modeler outputs to train probabilistic neural networks for unexploded ordnance (UXO) classification in magnetometry surveys. *IEEE Trans. Geosci. Remote Sens.* **2001**, *39*, 797–804. [CrossRef]
6. Jin, X.; Srinivasan, D.; Cheu, R.L. Classification of freeway traffic patterns for incident detection using constructive probabilistic neural networks. *IEEE Trans. Neural Netw.* **2001**, *12*, 1173–1187. [CrossRef]
7. Tan, K.H. Squirrel-cage induction generator system using wavelet Petri fuzzy neural network control for wind power applications. *IEEE Trans. Power Electron.* **2016**, *31*, 5242–5254. [CrossRef]
8. Kaur, K.; Rana, R.; Kumar, N.; Singh, M.; Mishra, S. A colored petri net based frequency support scheme using fleet of electric vehicles in smart grid environment. *IEEE Trans. Power Syst.* **2016**, *31*, 4638–4649. [CrossRef]
9. Wang, P.L.; Ma, L.; Goverde, R.M.P.; Wang, Q.Y. Rescheduling trains using petri nets and heuristic search. *IEEE Trans. Intell. Transp. Syst.* **2016**, *17*, 726–735. [CrossRef]
10. Farrag, M.E.A.; Putrus, G. Design of an Adaptive Neurofuzzy Inference Control System for the Unified Power-Flow Controller. *IEEE Trans. Power Deliv.* **2012**, *27*, 53–61. [CrossRef]
11. Ajami, A.; Shotorbani, A.M.; Aagababa, M.P. Application of the direct Lyapunov method for robust finite-time power flow control with a unified power flow controller. *IET Gener. Transm. Distrib.* **2012**, *6*, 822–830. [CrossRef]
12. Verveckken, J.; Silva, F.; Barros, D.; Driesen, J. Direct Power Control of Series Converter of Unified Power-Flow Controller with Three-Level Neutral Point Clamped Converter. *IEEE Trans. Power Deliv.* **2012**, *27*, 53–61. [CrossRef]
13. Jiang, S.; Gole, A.M.; Annakkage, U.D.; Jacobsoni, D.A. Damping Performance Analysis of IPFC and UPFC Controllers Using Validated Small-Signal Models. *IEEE Trans. Power Deliv.* **2011**, *26*, 446–454. [CrossRef]
14. Wang, L.; Chen, Z.J. Stability Analysis of a Wave-Energy Conversion System Containing a Grid-Connected Induction Generator Driven by a Wells Turbine. *IEEE Trans. Energy Convers.* **2010**, *25*, 555–563. [CrossRef]
15. Murthy, B.K.; Rao, S.S. Rotor side control of Wells turbine driven variable speed constant frequency induction generator. *J. Electr. Power Compon. Syst.* **2005**, *33*, 587–596. [CrossRef]
16. Cashman, D.P. Electrical Machine Characterisation and Analysis for Renewable Energy Applications. Ph.D. Thesis, University College Cork, Cork, Ireland, 2010.

17. Guo, J.; Crow, M.L.; Sarangapani, J. An Improved UPFC Control for Oscillation Damping. *IEEE Trans. Power Syst.* **2009**, *24*, 288–296. [CrossRef]
18. Mishra, S. Neural-network-based adaptive UPFC for improving transient stability performance of power system. *IEEE Trans. Neural Netw.* **2006**, *17*, 461–470. [CrossRef]
19. Wang, L.; Truong, D.N. Dynamic Stability Improvement of Four Parallel-Operated PMSG-Based Offshore Wind Turbine Generators Fed to a Power System Using a STATCOM. *IEEE Trans. Power Deliv.* **2013**, *28*, 111–119. [CrossRef]
20. Uddin, W.; Zeb, N.; Zeb, K.; Ishfaq, M.; Khan, I.; Ul Islam, S.; Tanoli, A.; Haider, A.; Kim, H.-J.; Park, G.-S. A Neural Network-Based Model Reference Control Architecture for Oscillation Damping in Interconnected Power System. *Energies* **2019**, *12*, 3653. [CrossRef]
21. Lin, F.J.; Liao, Y.H.; Lin, J.R.; Lin, W.T. Interior Permanent Magnet Synchronous Motor Drive System with Machine Learning-Based Maximum Torque per Ampere and Flux-Weakening Control. *Energies* **2021**, *14*, 346. [CrossRef]
22. Tan, K.H.; Lin, F.J.; Chen, J.H. A Three-Phase Four-Leg Inverter-Based Active Power Filter for Unbalanced Current Compensation Using a Petri Probabilistic Fuzzy Neural Network. *Energies* **2017**, *10*, 2005. [CrossRef]
23. Lin, F.J.; Lu, K.C.; Ke, T.H.; Li, H.Y. Reactive power control of three-phase PV system during grids faults using Takagi-Sugeno-Kang probabilistic fuzzy neural network control. *IEEE Trans. Ind. Electron.* **2015**, *62*, 5516–5528. [CrossRef]
24. Lin, Y.L.; Hsieh, J.G.; Jeng, J.H.; Cheng, W.C. On least trimmed squares neural networks. *Neurocomputing* **2015**, *161*, 107–112. [CrossRef]
25. Liao, S.H.; Han, M.F.; Chang, J.Y.; Lin, C.T. Study on adaptive least trimmed squares fuzzy neural network. *Int. J. Fuzzy Syst.* **2013**, *15*, 326–334.
26. Wang, L.; Li, H.W.; Wu, C.T. Stability analysis of an integrated offshore wind and seashore wave farm fed to a power grid using a unified power flow controller. *IEEE Trans. Power Syst.* **2013**, *28*, 2211–2221. [CrossRef]
27. Wang, L.; Zeng, S.Y.; Feng, W.K.; Prokhorov, A.V.; Mokhlis, H.; Huat, C.K.; Tripathy, M. Damping of Subsynchronous Resonance in a Hybrid System with a Steam-Turbine Generator and an Offshore Wind Farm Using a Unified Power-Flow Controller. *IEEE Trans. Ind. Appl.* **2021**, *57*, 110–120. [CrossRef]
28. Wang, L.; Nguyen Thi, M.S. Stability enhancement of large-scale integration of wind, solar, and marine-current power generation fed to an SG-based power system through an LCC-HYDC link. *IEEE Trans. Sustain. Energy* **2014**, *5*, 160–170. [CrossRef]
29. He, P.; Arefifar, S.A.; Li, C.; Wen, F.; Ji, Y.; Tao, Y. Enhancing Oscillation Damping in an Interconnected Power System with Integrated Wind Farms Using Unified Power Flow Controller. *Energies* **2019**, *12*, 322. [CrossRef]
30. Abbas, S.R.; Kazmi, S.A.A.; Naqvi, M.; Javed, A.; Naqvi, S.R.; Ullah, K.; Khan, T.-U.-R.; Shin, D.R. Impact Analysis of Large-Scale Wind Farms Integration in Weak Transmission Grid from Technical Perspectives. *Energies* **2020**, *13*, 5513. [CrossRef]
31. Wang, L.; Truong, D.N. Stability enhancement of DFIG-based offshore wind farm fed to a multi-machine system using a STATCOM. *IEEE Trans. Power Syst.* **2013**, *28*, 2882–2889. [CrossRef]
32. Joshi, M.; Sharma, G.; Bokoro, P.N.; Krishnan, N. A Fuzzy-PSO-PID with UPFC-RFB Solution for an LFC of an Interlinked Hydro Power System. *Energies* **2022**, *15*, 4847. [CrossRef]